Lattice dynamics, phase transitions and hydrogen effective charges of betaine phosphite: a comparison with betaine phosphate and their deuterated analogues

1998 J. Phys.: Condens. Matter 10 6147

(http://iopscience.iop.org/0953-8984/10/27/015)

J. Phys.: Condens. Matter **10** (1998) 6147–6169. Printed in the UK PII: S0953-8984(98)91075-X

Lattice dynamics, phase transitions and hydrogen effective charges of betaine phosphite: a comparison with betaine phosphate and their deuterated analogues

M L Santos†, A Almeida†, J Agostinho Moreira†, M R Chaves†, A Klöpperpieper‡ and F Gervais§

† Departamento de Física da Faculdade de Ciências, Universidade do Porto, Rua do Campo Alegre, 687, P-4150 Porto, Portugal

‡ Fachbereich Physik der Universität der Saarlandes, 66041 Saarbrücken, Germany

§ Laboratoire d'Electrodynamique des Matériaux Avancés, Faculté des Sciences et Techniques, Université François Rabelais, F-37200 Tours, France

Received 27 February 1998, in final form 2 April 1998

Abstract. The temperature dependence of complete infrared reflection spectra of a betaine phosphite single crystal is reported for the polarizations parallel to $\boldsymbol{a}$ and $\boldsymbol{b}$ axes in the wavenumber range from 10 to 5000 cm^{-1}. They are compared with previous data that were limited to the range 10–600 cm^{-1}. They are also compared with reflectivity spectra of betaine phosphate, betaine arsenate, deuterated betaine phosphite single crystals and betaine compressed powder. These comparisons allow a mode assignment. Spectra were fitted with the factorized form of the dielectric function. The role of phonons in the behaviour of the dielectric constant in the vicinity of the ferroelectric (FE)–paraelectric (PE) phase transition is discussed. The decrease of effective charges along the FE axis below the FE–PE phase transition is assigned to an increase of oxygen–hydrogen electronic orbital hybridization related to the change of average bond-length.

1. Introduction

Betaine phosphite (BPI)—$(CH_3)_3NCH_2COOH_3PO_3$—and betaine phosphate (BP)—$(CH_3)_3NCH_2COOH_3PO_4$—show a wide variety of chemical bondings: ionic, covalent, hybridized, hydrogen bonds and Van der Waals (due to the large oxygen polarizability). They are built up from the betaine molecule and the inorganic units of phosphites and phosphates, respectively, linked by hydrogen 'bridges'. Betaine phosphite and phosphate, both pure and mixed compounds ($BP_{1-x}BPI_x$), present a wide range of interesting and complex dielectric properties which are related to ferroelectric behaviour on the one hand, and to the specific chemical arrangement on the other hand. In addition to the potential role of chemical and structural parameters, another important question concerns the role of the dynamics, more specifically that of the hydrogen atoms which link the organic molecule to PO_4^{3-} ions in BP and HPO_3^{2-} ions in BPI. This is not indeed the sole iono-covalent crystalline system that displays an interesting sequence of structural phase transitions. Systems of the KDP family (potassium dihydrogen phosphate) like $NH_4H_2PO_4$, RbH_2PO_4, $NH_4H_2AsO_4$ and mixed crystals $Rb_{1-x}(NH_4)_xH_2PO_4$, currently known as RADP, display interesting physical phenomena also. The hydrogen atoms (often referred to as 'protons') of the O–H$\cdots$O bonds in BP and BPI supposedly play an important role in

0953-8984/98/276147+23$19.50

the low-temperature phase transitions, as can be checked by the effect of deuteration on the phase transition temperatures. A similar phenomenon is observed in compounds of the KDP family. However, the relation is not straightforward. For example, it was shown in RbH_2PO_4 that the *coupling* of PO_4 vibrations with those of the O–H$\cdots$O bonds is responsible for the spontaneous polarization found oriented in a direction *perpendicular* to that of the O–H$\cdots$O bonds [1–3]. It is interesting, therefore, to check whether such a coupling takes place in betaine compounds in which the symmetry of the inorganic pyramidal groups HPO_3 is modified with respect to the tetrahedra which are present in all KDP compounds and BP too. On the other hand, just like in RADP, there have been found manifestations of frustration phenomena in ($BP_{1-x}BPI_x$) stemming from ferro- and antiferroelectric competitive interactions.

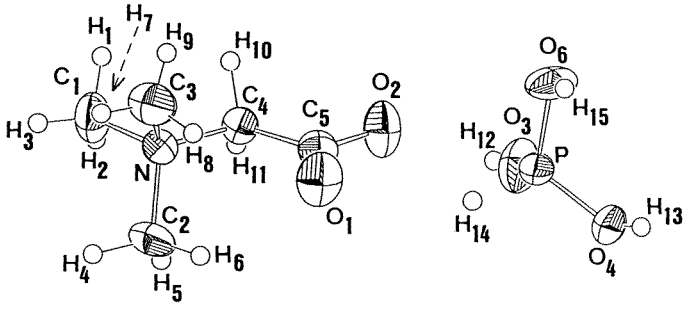

Figure 1. Room temperature structure of betaine phosphite.

The structure of one betaine phosphite unit is reproduced in figure 1. The inorganic groups in BP and BPI are linked by hydrogen bonds (H_{13}, H_{15}) forming zig-zag-like chains along the [010] axis. The betaine molecules are oriented almost perpendicularly to the chains (mainly along the [100] direction) and are linked to the PO_3^{3-} ions by one hydrogen bond in BPI or to the PO_4^{3-} ions by two hydrogen bonds in BP [4, 5]. This difference yields a drastic change of properties and since deuteration largely shifts the transition temperature, by $\sim$70 K in BP [6] and by $\sim$100 K in BPI [7], proton dynamics is suspected to play a leading role in the physics of these systems. The same situation prevails in KDP-type compounds. BPI is known to present two structural phase transitions [8, 9]: at $T_1 = 355$ K, from a paraelectric $P12_1/m1$ high-temperature phase to an antiferrodistorsive $P12_1/c1$ phase with a simultaneous doubling of the unit cell along the $\boldsymbol{c}$ axis, and an order–disorder phase transition to a ferroelectric $P12_11$ phase occurring at $T_2 = 220$ K. ENDOR measurements [10] established that the phase transition at T_2 is related to a dynamic proton ordering in the two hydrogen bonds linking each PO_3 group to its chain neighbours. An x-ray study evidenced the existence of a strong anisotropy in BPI [9, 11].

Infrared reflection spectroscopy is able to probe polar species and gives access to a wide frequency range. This technique is expected, therefore, to be useful since the relevant susceptibility in the $BP_{1-x}BPI_x$ lattice instabilities is the complex dielectric function ε. A previous work on BP [12] has shown the power, but also the limits, of this method of dielectric spectroscopy. The limitations partially stem from the very large number of modes, some of them being very broad. Weak modes were shown to interfere with broad modes due to coupling in the Fano sense [13], and give very asymmetric mode profiles. Similar spectral species were observed in the spectra of the parent RADP family, *viz.* $NH_4H_2PO_4$, RbH_2PO_4 and mixed crystals $Rb_{1-x}(NH_4)_xH_2PO_4$ [1–3]. By comparison with the RADP

family, the study of BP [12] has exemplified the problems related to generalized mode–mode coupling. In particular, the limits of the mode assignment have been shown in the case of coupled mixed modes. Also, a dielectric constant anomaly was shown to have its origin in the temperature dependence of a set of low-frequency coupled modes and not from a single soft mode. These phenomena makes the data analysis more complicated, but it is however worth doing it in systems, even complex, where the relevant susceptibility is dielectric and is expected to be at least partly influenced by atomic motions of charged species in the infrared frequency range. The present study performed in the complete frequency range from 10 to 5000 cm^{-1}, complements previous studies published by Koch and Happ [14] and by Ebert *et al* [15] in the limited range 10–600 cm^{-1} as well as by Baran *et al* [16] who interpreted Raman and infrared absorption data obtained in the paraelectric phase of BPI (frequency range 400 to 3100 cm^{-1}).

Another advantage of infrared reflectivity spectroscopy is the capability to probe the effective ionic charges that are related to the chemical bonding and its eventual evolution at a structural phase transition. This might be interesting in complex compounds like betaine phosphite where virtually all kinds of bonding are present. Previous studies performed in ferroelectric systems evidenced significant evolution of the chemical bonding along the ferroelectric axis [17]. A drastic change of ionic effective charge was also found at an insulator–metal phase transition, with the same technique [18].

2. Experiment

The samples were prepared in a similar way to the one referred to in [12]. One platelet with a face of 9×7 mm^2 containing both *a* and *b* axes was studied with the same technique and in the same conditions referred to in [12].

2.1. Phonons

2.1.1. Data reduction. Spectra can be Kramers–Krönig transformed to obtain the dielectric response but this treatment may introduce errors [19]. This treatment may be complemented by a fit of the dielectric function model

$$\varepsilon(\omega) = \varepsilon_\infty \prod_j \frac{\Omega_{jLO}^2 - \omega^2 + \mathrm{i}\gamma_{jLO}\omega}{\Omega_{jTO}^2 - \omega^2 + \mathrm{i}\gamma_{jTO}\omega} \tag{1}$$

to reflectivity data via

$$R(\omega) = \left| \frac{\sqrt{\varepsilon(\omega)} - 1}{\sqrt{\varepsilon(\omega)} + 1} \right|^2. \tag{2}$$

In equation (1), the subscripts TO and LO refer to transverse and longitudinal optical modes, respectively. The Ω represent frequencies and γ mode dampings (linewidth at half maximum). The dielectric function model (1) is preferred to the more conventional summation over Lorentz oscillators for the reasons detailed in the review paper [18]. The factorized form of the dielectric function was successfully used to fit the spectra of compounds displaying parent properties, e.g. RbDP [1–3], and BP [12]. For the case of BPI too, the model (1) appears to be the simplest one which is able to fit the data satisfactorily. Indeed, we will see that certain regions of the spectra display heavily damped modes which are internal to the HPO_3 pyramids and which are coupled with proton motions. These broad modes show up in the same spectral regions as some of those of the betaine molecules that appear as very narrow lines. As a result, two neighbour TO and LO oscillators may exhibit

very different damping terms γ. This is just the situation in which the factorized form of the dielectric function (1) is the most relevant because it does not implicitly assume the same damping for two neighbour TO and LO modes as the more usual summation model does, as detailed in [19]. In particular, this situation may give rise to asymmetric phonon lines that result from coupling of a narrow line with a broad continuum, and the factorized form (1) is able to describe the line profiles satisfactorily in this case, as shown in [1–3] and [12] for example.

Once the spectrum is fitted with two adjustable parameters (frequency and damping) per mode (TO or LO), individual oscillator strengths $\Delta\varepsilon_j$ may be deduced from the TO–LO splittings via

$$\frac{\Delta\varepsilon_j}{\varepsilon_\infty} = \Omega_{jTO}^{-2}\left(\prod_k(\Omega_{kLO}^2 - \Omega_{jTO}^2)\right)\left(\prod_{k\neq j}(\Omega_{kTO}^2 - \Omega_{jTO}^2)\right)^{-1}. \tag{3}$$

Oscillator strengths indeed are important parameters in this study because they amount to the contribution of an individual mode to the dielectric constant.

Infrared reflection spectra for the polarizations parallel to both $\boldsymbol{a}$ and $\boldsymbol{b}$ axes are shown in figures 2 and 3 for both extreme temperatures investigated. Our data compare reasonably well with previously published data in a limited spectral range [15] if one accounts for the

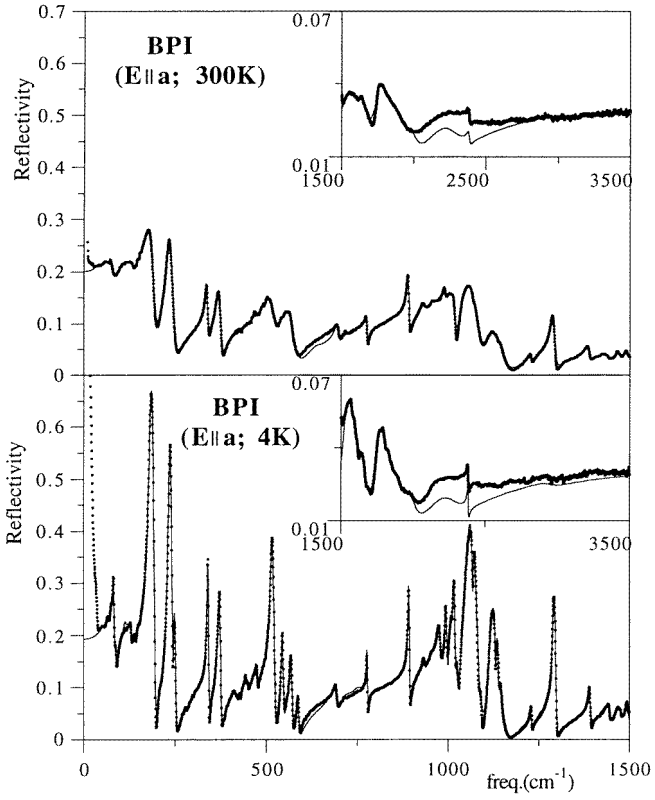

Figure 2. Examples of best fits (thin lines) of the dielectric function model (1) to infrared reflection spectra (dots) at two extreme temperatures investigated (4 K and 300 K), for the polarization parallel to the $\boldsymbol{a}$ axis.

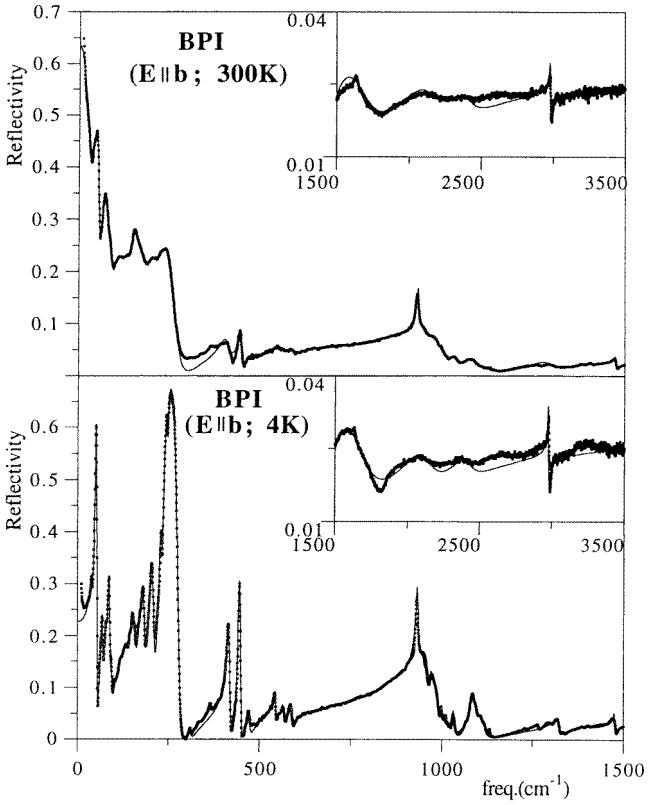

Figure 3. Examples of best fits (thin lines) of the dielectric function model (1) to infrared reflection spectra (dots) at two extreme temperatures investigated (4 K and 300 K), for the polarization parallel to the $\boldsymbol{b}$ axis.

fact that [15] refers to a BPI compound doped with BP. Note that for BPI ($\boldsymbol{E}\|\boldsymbol{a}$) at 4 K, the far-infrared radiation is reflected upon the sample holder inside the cryostat in the spectral region where the sample is transparent, *viz.* below 50 cm^{-1}. The 'rich structure' reported in [15] below 35 cm^{-1} for the polarization $\boldsymbol{E}\|\boldsymbol{a}$ most likely corresponds to interference fringes in a semi-transparent regime, and not to phonons.

Spectra have been recorded at five intermediate temperatures. All reflectivity spectra have been fitted with (1) and (2). Examples of agreement between model and experiment are shown in figures 2 and 3. It is seen that the parameter that appears the most sensitive to the T_2 phase transition is the oscillator strength of the modes, at least when their frequency is lower than 600 cm^{-1}. When their frequency is higher, the oscillator strength does not vary much with temperature, within experimental error.

2.1.2. Tentative mode assignment. The results obtained from factor group analyses of BPI in its different phases are summarized in table 1. The number of modes used in the fit of the reflectivity data below T_1 ($<$38 modes for $\boldsymbol{E}\|\boldsymbol{b}$ and $<$76 modes for $\boldsymbol{E}\|\boldsymbol{a}$) is lower than the corresponding number calculated from group theory analyses. The good fits obtained seem to indicate that the unconsidered infrared active modes play a less important role in the infrared spectra of BPI because they are too weakly polar. The breaking of symmetry

Table 1. Factor group analysis in the various phases of BPI and optical activities.

$T_1 = 355$ K			$T_2 = 220$ K					
$P2_1/m$			$P2_1/c$			$P2_1$		
Number of modes	Species	Optical activity	Number of modes	Species	Optical activity	Number of modes	Species	Optical activity
43	A_g	R	75	A_g	R	155	A	R, IR
32	B_g	R	75	B_g	R			
34	A_u	IR	80	A_u	IR	154	B	R, IR
44	B_u	IR	79	B_u	IR			

Table 2. Mode frequency and profile observed in some phosphite compounds (vs, very strong; s, strong; m, medium; w, weak; vw, very weak; d, depolarized; p, polarized; b, broad; sh, sharp) [20].

Raman	IR		
Na_2HPO_3 (aq. sol)	K_2HPO_3 (aq. sol)	$BaHPO_3$ (cryst. in Nujol)	Assignment
459 (m) d	465 (m) b	471 (m)	E PO_3
		498 (m)	asym. deformation
550 (vw)	567 (m)	591 (m)	A_1PO_3
			sym. deformation
993 (s) p	979 (m) sh	977 (m) sh	A_1PO_3
			sym. stretching
1032 (m) d	1027 (vw) b	1066 (w) sh	E PH
		1021 (w) sh	def.
1100 (vw)	1085 (vs) b	1083 (vs) b	E PO_3
		1110 (vs) b	def.
2330 (s) p	2315 (m) sh	2410 (m) sh	A_1PH stret.

at T_2 is witnessed by the appearance of some modes in the ferroelectric phase below T_2, as will be seen in due course. These new modes derive from modes which are Raman active in the high temperature phase and are of type B_g for polarization $\boldsymbol{E}\|\boldsymbol{a}$ and A_g for polarization $\boldsymbol{E}\|\boldsymbol{b}$. To emphasize the origin of the modes observed in the ferroelectric phase, we chose to maintain the high-temperature notation as usually done in current literature.

It is instructive to compare the infrared spectrum of BPI with those of BP, BA and betaine to present an assignment of vibrational modes. We have taken into consideration the frequencies of the modes internal to the HPO_3^{2-} molecular ion given in table 2 [20]. TO modes of both compounds at 4 K are compared in figures 4(i) to (iii), for polarizations $\boldsymbol{E}\|\boldsymbol{a}$ and $\boldsymbol{E}\|\boldsymbol{b}$ in BP and BPI, and for $\boldsymbol{E}\|\boldsymbol{a}$ and $\boldsymbol{E}\|\boldsymbol{c}$ in BA. The function displayed in figure 4 is the imaginary part of the dielectric response deduced from the best fit to reflectivity spectra of BPI and BP, and from Kramers–Krönig transformed BA and betaine reflectivity spectra. The displayed assignment will be discussed in detail later on. Furthermore, a comparison of BPI with preliminary results obtained on partially deuterated BPI, here labelled DBPI, is shown in figures 5 and 6. The comparison is made with Kramers–Krönig transformed DBPI data to avoid an additional fitting procedure which is a formidable task when the number of modes is so large, and which is not needed when the purpose is the comparison of peak positions and spectra profiles.

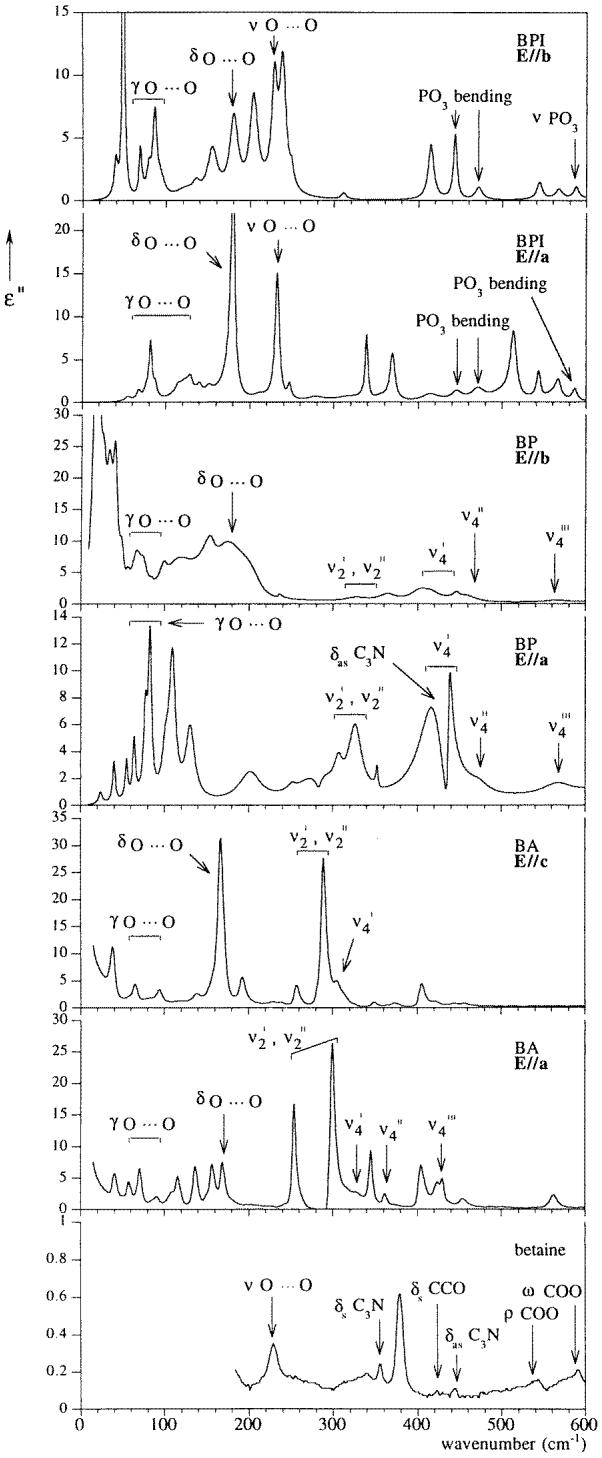

Figure 4. A comparison of the imaginary part of the dielectric function at 4 K of betaine phosphite (BPI), betaine phosphate (BP) [12], betaine arsenate (BA) [26] and compacted betaine powder [20, 26], showing the response of transverse optical modes for the polarizations indicated.

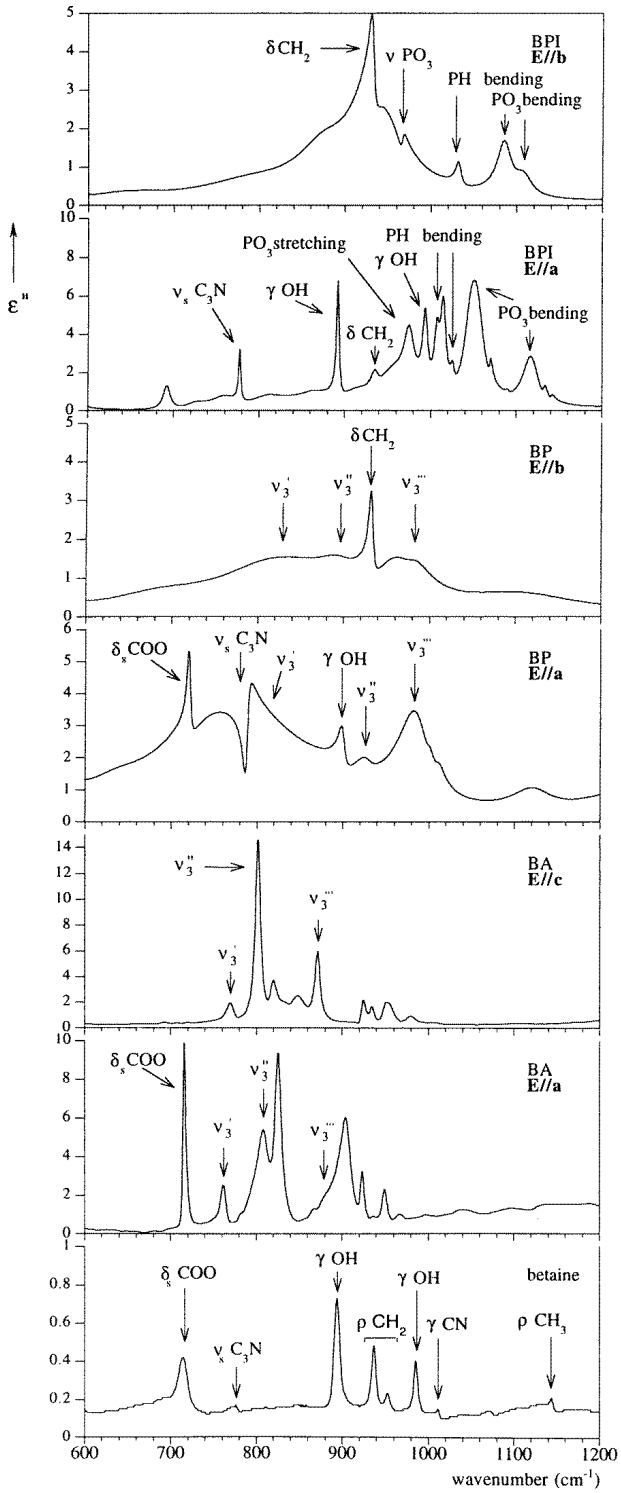

Figure 4. (Continued)

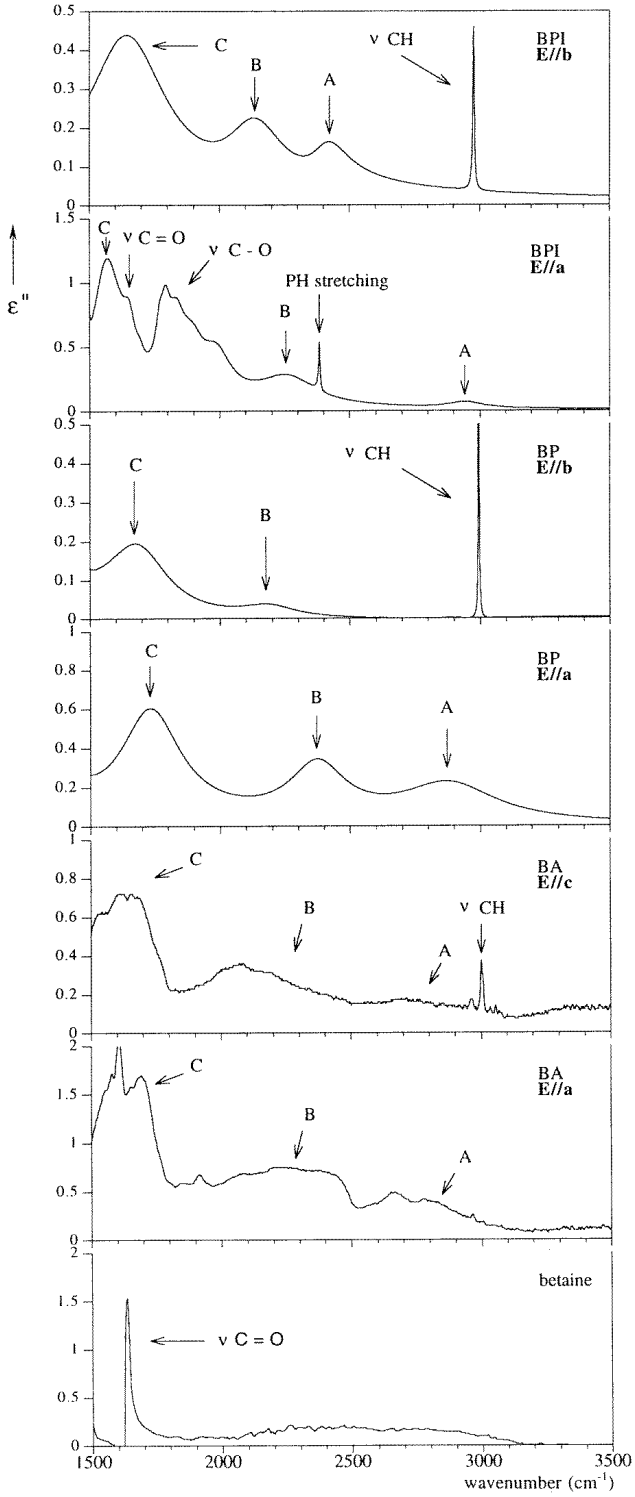

Figure 4. (Continued)

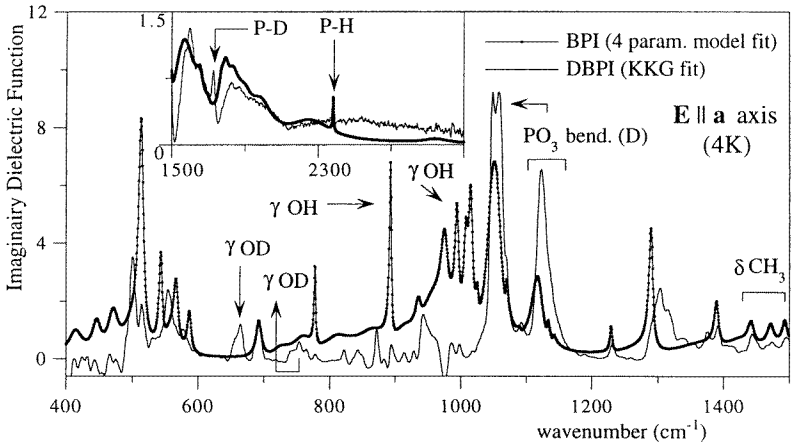

Figure 5. A comparison of hydrogenated (line with points) and deuterated (thin line) betaine phosphite for the polarization parallel to the $\boldsymbol{a}$ axis.

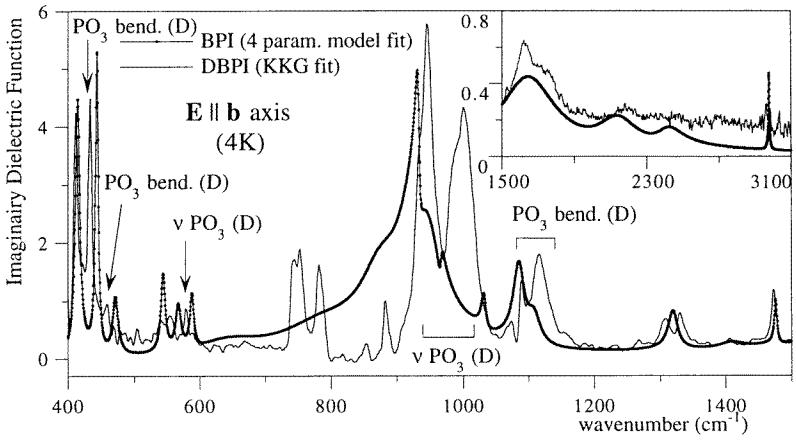

Figure 6. Same as legend to figure 5 for the polarization parallel to the $\boldsymbol{b}$ axis.

Prior to the discussion which follows this paragraph it is worth emphasizing a few characteristical features of the BP/BPI and BPI/DBPI comparisons. The BP/BPI difference appears considerable and not restricted to the specific spectral range of the modes internal to the phosphate and phosphite species. The region of external modes below 300 cm^{-1} is strongly modified in the phosphite compound also. However, the spectra below 300 cm^{-1} in BPI are made up of a sum of nearly symmetric peaks, whereas it is not so for BP, so that the latter appears to be the abnormal one actually. On the other hand, the differences of BPI/DBPI appear also considerable. Our previous data [12] concerning the comparison BP/DBP are reproduced in figure 7 to complement the new available data.

To arrive at a mode assignment, proposed for BPI in figures 4 to 10 and in table 3, the following arguments were used.

(a) A C–H stretching mode of the betaine molecule peaks very near 2999 cm^{-1} in BPI, BP and BA, as expected in any compound containing this bond [21]. It is little affected by

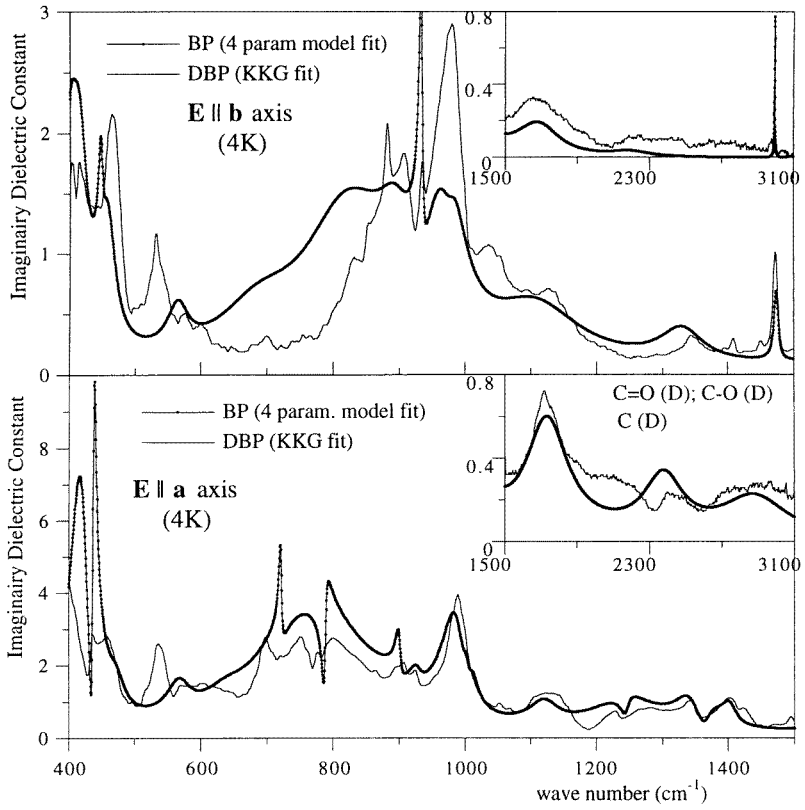

Figure 7. A comparison of hydrogenated (line with points) and deuterated (thin line) betaine phosphate for the polarization parallel to the $\boldsymbol{b}$ axis (top) and $\boldsymbol{a}$ axis (bottom).

the crystal field, as its frequency remains almost unchanged in BA, BP and BPI (figure 4(iii)). The peak is sharp for the polarization parallel to the $\boldsymbol{b}$ axis in both BPI and BP and for the polarization parallel to the $\boldsymbol{c}$ axis in BA, i.e. parallel to the chains (figure 4(iii)).

(b) The sharp P–H stretching mode is observed parallel to the $\boldsymbol{a}$ axis near 2350 cm^{-1} (figure 4(iii)), as expected from table 2. No signature is found in the $\boldsymbol{b}$ direction, consistent with the orientation of the P–H bond nearly along $\boldsymbol{a}$ in the (a, c) plane. Its frequency is considerably downshifted in the deuterated compound as may be expected from the ratio of effective masses (inset in figure 5).

(c) In the spectral range 1500–3500 cm^{-1} (figure 4(iii)), the broad A, B and C bands of the stretching mode ν_{OH} are clearly visible and their frequency range is in agreement with the one found in compounds like KDP [1, 3] and TDA [22]. In BPI, for the polarization $\boldsymbol{E}\|\boldsymbol{b}$, the three bands are closer together in frequency than for the polarization $\boldsymbol{E}\|\boldsymbol{a}$. This occurrence can be explained by the existence of stronger hydrogen bonds in the $\boldsymbol{b}$ direction than in the $\boldsymbol{a}$ direction [23]. Reinforcing this assertion, x-ray data [11] show that in BPI the O_4–$H_{13}\cdots O_4$ bond (parallel to the $\boldsymbol{b}$ axis) is shorter than O_6–$H_{15}\cdots O_6$ or O_2–$H_{12}\cdots O_3$ (which roughly belong to the (a, c) plane), while in BP and BA, the three bonds have very similar lengths. Nevertheless, because this frequency region was particularly difficult to fit, specially around 2500 cm^{-1}, some weak and broad modes have not been considered. Consequently the true spectrum profiles in this frequency range actually present a more

Table 3. Tentative assignment of vibration modes in BPI.

Ω_{TO} (cm^{-1})		Mode assignment
$E\|a$	$E\|b$	
68–88	69–93	$\gamma_{O\cdots O}$
172	180	$\delta_{O\cdots O}$
233	229	$\nu_{O\cdots O}$
446	443	PO_3 asym. bend.
471	471	PO_3 asym. bend.
587	588	PO_3 sym. bend.
778	—	ν_{sC_3N}
892	—	γ_{OH}
936	932	δ_{CH_2}
976	966	PO_3 sym. stretch.
994	—	γ_{OH}
1006	—	PH bending
1026	1032	PH bending
1050	1086	PO_3 sym. bend.
1117	1108	PO_3 asym. bend.
1565	1650	ν_{OH} (C band)
1655	—	$\nu_{C=O}$
1770–2000	—	ν_{C-O}
2260	2130	ν_{OH} (B band)
2383	—	PH stretching
2964	2410	ν_{OH} (A band)
—	2977	ν_{CH}

complex structure than the three A, B, C bands. This occurrence has been identified with the existence of a strong coupling to the lattice and with tunnelling effects [24].

(d) In BP and BA, the C–O, C=O bonds of the carboxyl group do not appear to yield specific signatures in the BP spectra. The respective band(s) could be hidden under the C band or be so weak that may have been neglected in the fit of the BP reflectivity spectra [12]. The comparison with DBP shows a more complex spectrum profile for the DBP that may probably be due to a shift of the C band and a consequent better visualization of the C–O, C=O bands. This is seen in the inset of figure 7 for $\boldsymbol{E}\|\boldsymbol{a}$. In BPI, only one bond links the HPO_3^{2-} ion to the betaine. Consequently, the C–O and C=O modes are then distinguishable and can be clearly differentiated (figure 4(iii)).

(e) The assignment of all PO_3^{3-} modes presented in table 2 and in figures 4(i) and 4(ii) was done considering both the intensity and the frequency of the modes tabulated in table 3, as well as accounting for the raising of the degeneracy due to the crystal field. In the present assignment, the two PO_3^{3-} bending modes at ≈1050 and 1117 cm^{-1} for $\boldsymbol{E}\|\boldsymbol{a}$ are strong and broad as expected. The agreement is just as good for the three PO_3^{3-} bending modes found in the range ≈443–588 cm^{-1}, as they are weaker and sharper than the higher-frequency ones. However, for $\boldsymbol{E}\|\boldsymbol{b}$ no mode appears at 1050 cm^{-1} as in the polarization parallel to the $\boldsymbol{a}$ axis. The best candidate is the indicated mode at ≈1080 cm^{-1}. In fact, although the difference between frequencies of the assigned mode in both polarizations is ≈30 cm^{-1}, this amounts to only 3% of its value. On the other hand, the temperature variation of the oscillator strength in both polarizations present a minimum at T_2, reaching a relative maximum around 100 K and subsequently decreasing (figures 8(ii) and 9(iii)). These modes are somewhat affected by deuteration as can be seen in figures 5 and 6.

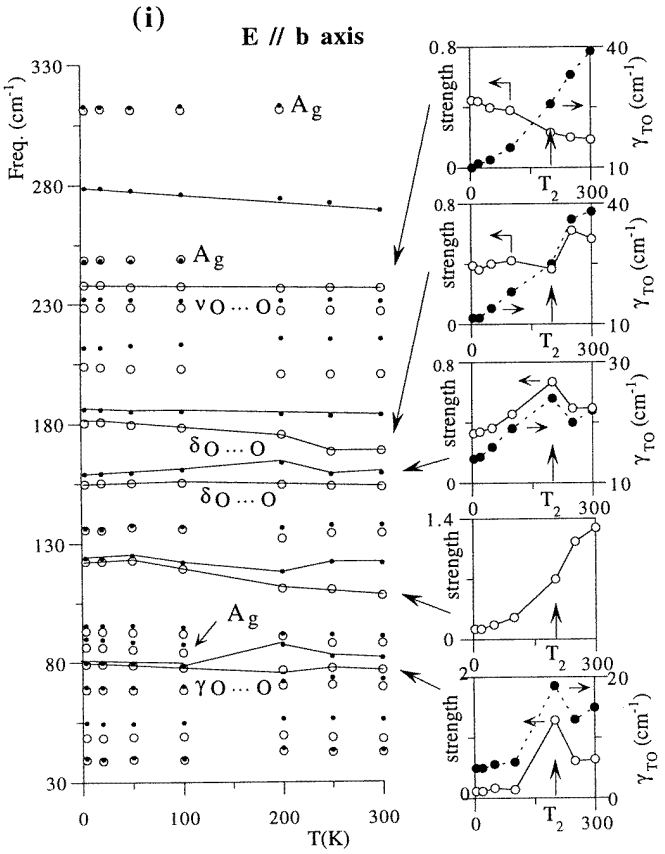

Figure 8. Temperature dependence of TO (open symbols) and LO (full symbols) modes in betaine phosphite for the polarization parallel to the ***b*** axis. Insets show the temperature dependence of the damping γ_{jTO} and of the dielectric strength $\Delta\varepsilon_{jTO}$ related to TO and LO mode frequencies via (3).

(f) The tentative assignment in BP of bending ν_2 and ν_4 and stretching ν_3 internal modes of the PO_4^{3-} ion relies on the comparison with the fundamental vibrational frequencies of the free phosphate tetrahedron as well as with the corresponding bands previously assigned in BA [25] and KDP [1, 2, 22] type compounds. The observed upshift of these bands in BP as referred to BA (due to smaller mass of the phosphate atom) reinforces the proposed assignment.

It should be noted that the assignment of the ν_2, ν_4 modes in BA (stemming from Raman [25] and IR [26] studies) shows a slightly higher intensity for the ν_2 modes as compared to the ν_4 modes. This seems unexpected, as the ν_2 modes are more weakly polar in the free ion. But if we consider table 4 [4, 27] in which it is clear that the inorganic AsO_4^{3-} deforms more easily due to its larger size than the PO_4^{3-}, a stronger electric dipole momentum is expected due to the crystal field.

(g) Referring to the work of Ouafik [22], the external modes $\gamma_{O\cdots O}$, $\delta_{O\cdots O}$ and $\nu_{O\cdots O}$ are expected to be visible at the low frequency range from 80 to 200 cm^{-1}. By comparing BP, BPI and BA spectra, we assign the $\gamma_{O\cdots O}$ and $\delta_{O\cdots O}$ modes in BP as the bands located at 60–100 cm^{-1} and 180 cm^{-1}, respectively. In BPI the modes $\gamma_{O\cdots O}$, $\delta_{O\cdots O}$ and $\nu_{O\cdots O}$ are assigned as presented in figure 4(i) and in table 2.

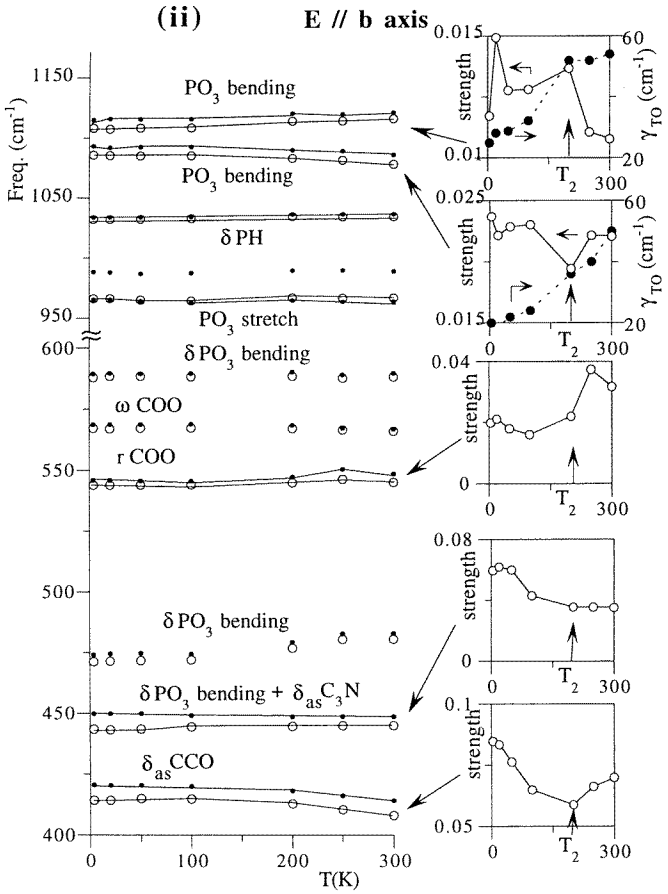

Figure 8. (Continued)

Table 4. Atomic distances in PO_4^{3-} and AsO_4^{3-} ions in BP and BA, respectively [4, 27].

Bond	Bond distance (Å) AsO_4^{3-}	Bond distance (Å) PO_4^{3-}	Bond
As–O_3	1.695(2)	1.533(2)	P–O_3
As–O_4	1.675(2)	1.532(2)	P–O_4
As–O_5	1.704(2)	1.567(2)	P–O_5
As–O_6	1.679(2)	1.533(2)	P–O_6

It should be noted that the assignments presented in items (a), (b) and (e) are in fair agreement with those of [16]. From all that has been said until this point we find this work a useful complement to the mode assignment presented in [16] regarding BPI's paraelectric phase.

Other modes show a more complex behaviour upon deuteration than the vibrations discussed above. Allowing for a systematic analysis one may consider three spectral regions, which will be discussed in the following: 400–600 cm^{-1}, 700–1200 cm^{-1} and the range above 1500 cm^{-1}. Nevertheless, it should be noted that some effects due to deuteration may be responsible for the 'richness' of the DBPI spectra, such as: the existence of anharmonici-

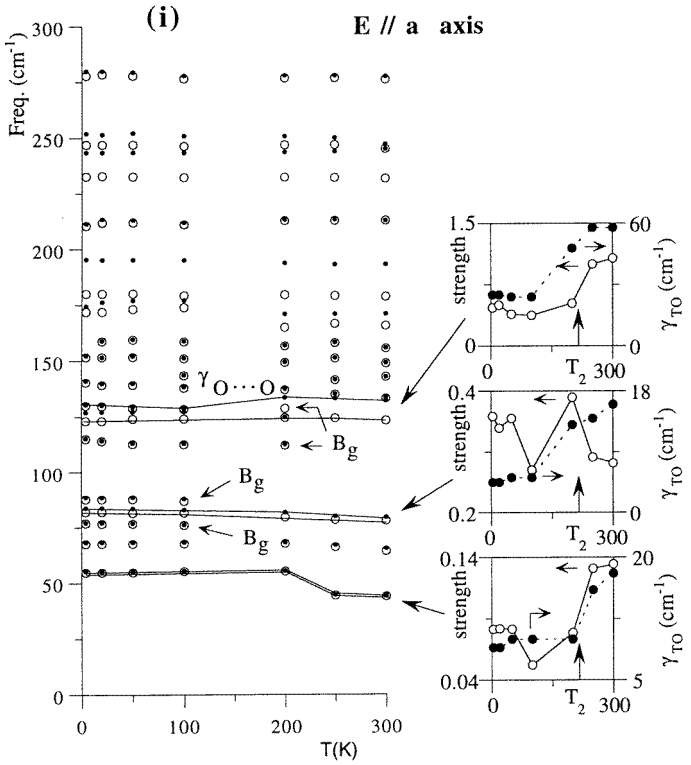

Figure 9. Temperature dependence of TO (open symbols) and LO (full symbols) modes in betaine phosphite for the polarization parallel to the $\boldsymbol{a}$ axis. Insets show the temperature dependence of the damping γ_{jTO} and of the dielectric strength $\Delta\varepsilon_{jTO}$ related to TO and LO mode frequencies via (3).

ties which lead to the appearance of harmonics or to oscillator combinations, the occurrence of geometric and mass effects due to the substitution of hydrogen by deuterium and also a certain amount of leakage of a number of bands into disallowed symmetry species [28].

(a) Above 1500 cm^{-1}, we observe in figure 5 the $\sqrt{2}$ downshift of the PH sharp mode upon deuteration.

(b) In the range 400–600 cm^{-1} (figures 5 and 6), the average frequency of the spectral weight is little affected by deuteration. The result is consistent with our interpretations above, that the vibrations in this range mainly involve PO_3 bending modes.

(c) In the range 700–1200 cm^{-1} (figures 5 and 6), very abnormal effects are observed upon deuteration. They appear as shifts of the spectral weight but may in fact be partly due to the energy transfer phenomena between coupled modes of different frequencies. Observing figure 6 such an energy transfer upon deuteration appears to occur in BPI, for $\boldsymbol{E}\|\boldsymbol{b}$, between the two bending modes around 1100 cm^{-1} and from modes in the region 800–900 cm^{-1} to those in 900–1000 cm^{-1}, which includes the PO_3 stretching mode that peaks in this frequency range. In figure 5 it can also be seen that PO_3 bending modes (1030–1080 cm^{-1}) have their intensity increased while neighbouring modes around 1000 cm^{-1} are weakened by deuteration. As some proton modes appear in this frequency range (figure 4(ii)) it is natural to conclude that these phenomena stem from the strong coupling between proton

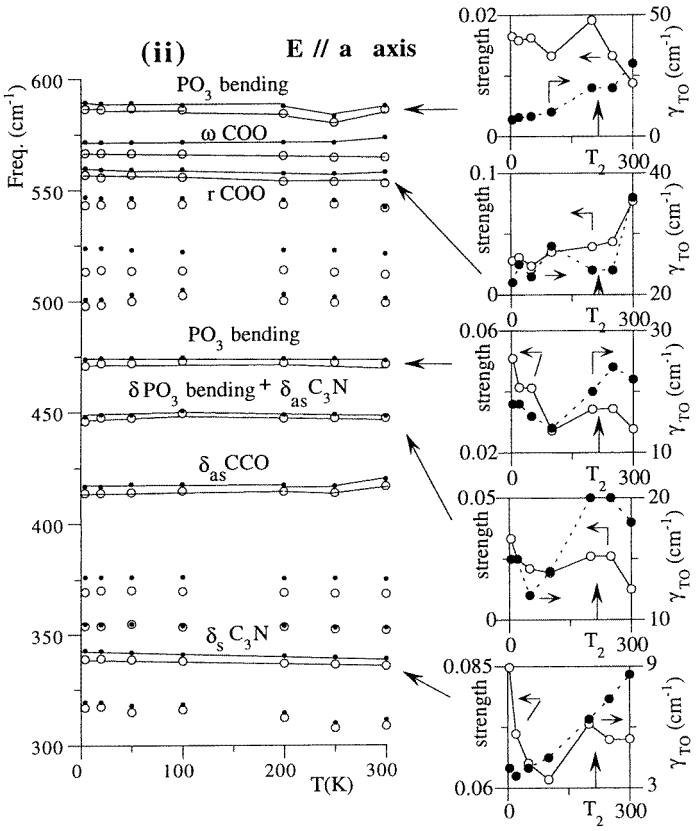

Figure 9. (Continued)

motions and the internal vibrations belonging to PO_3^{3-} ions. Then, modes would no longer behave like isolated modes and the spectra would result from the outcome of complex mode interactions. This behaviour is also observed in BP for $\boldsymbol{E}\|\boldsymbol{b}$, in the 650–1050 cm^{-1} frequency range (figures 4(ii) and 7), involving internal ν_3 and proton modes.

In figure 5 the low level of ε'' in the frequency range 400–500 cm^{-1} for $\boldsymbol{E}\|\boldsymbol{a}$ is due to the intrinsic low level of the reflectivity data in this polarization and because this frequency range is already in the validity limit of the used filter. In the frequency range 700–1000 cm^{-1} for $\boldsymbol{E}\|\boldsymbol{a}$ (figure 5) the ε'' level of DBPI is also too low. In the polarization parallel to the b direction this effect is less noticeable due to the strength of some modes in 700–800 cm^{-1}. We believe this is due to a defective surface recrystallization during the polishing of the DBPI samples, just prior to being analysed.

2.1.3. Mode couplings. In all spectra that consist of more than one excitation, the modes are coupled, the more so the nearer they are in frequency. There are two extreme behaviours of mode coupling: (i) discrete mode–mode coupling which manifests itself by level repulsion phenomena and (ii) interference of a discrete state with a broad continuum. The signature of the latter case is generally a strong asymmetry of the narrow line that may appear as a hole in the continuum instead of a peak in extreme cases. This is well described by the general Fano formalism [12]. Strong interference profiles of coupled narrow and

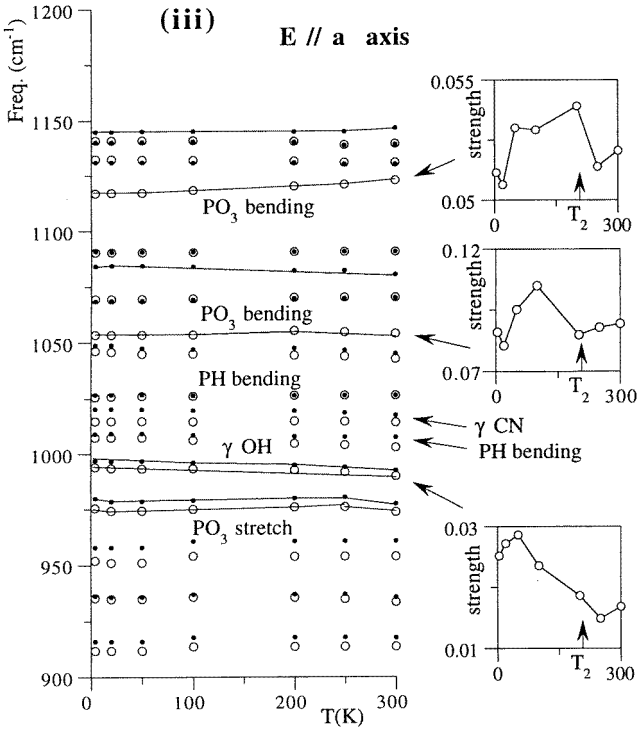

Figure 9. (Continued)

broad lines were observed in KDP-type crystal spectra. They were understood in terms of coupling of proton motions in the hydrogen bridges with internal degrees of freedom of the PO_4 tetrahedra [1–3]. This interpretation was substantiated by the observation of coupled proton–ν_4-mode softening that triggers the PE–FE phase transition. Upon inspection of results at 4 K in figure 4, what appears striking is just the existence of narrow and broad bands that interfere to give asymmetric profiles as shown for the ν_3 and ν_4 PO_4 mode groups in BP. This interference occurs between $\nu_s(C_3N)$ (narrow) and ν_3 (broad) bands (figure 4(ii)) and between $\delta_{as}(C_3N)$ (narrow) and ν_4 (broad) bands (figure 4(i)). Similar phenomena appear in BPI too, for example near 960 cm^{-1} for $\boldsymbol{E}\|\boldsymbol{b}$, still at 4 K (figure 4(ii)), but they are found to be much less marked than in BP and we have to wonder why. On the other hand, for the polarization parallel to the $\boldsymbol{a}$ axis, the spectrum of BPI at 4 K is almost 'normal', in that no asymmetric profiles are observed (figure 4). So, BPI appears to be intermediate between a 'normal' case and the very abnormal BP one. We have two experimental arguments to rank BPI in this sequence: peak asymmetries like the mode near 960 cm^{-1} and the energy transfer phenomena upon deuteration due to complex phenomena of couplings and softenings.

2.2. Dielectric constant

The low-frequency limit of a reflectivity spectrum is straightforwardly related to the dielectric constant (at 300 GHz) via (2). It is instructive to inspect its temperature dependence. This is obtained as $\varepsilon_0 = \varepsilon_\infty + \sum \Delta\varepsilon_j$ where the summation refers to all

phonon oscillator strengths; or equally well on setting $\omega = 0$ in (1) and using the generalized Lyddane–Sachs–Teller relationship

$$\varepsilon_0 = \varepsilon_\infty \prod_j \frac{\Omega_{jLO}^2}{\Omega_{jTO}^2}. \tag{4}$$

The temperature dependence of ε_0 at 300 GHz is plotted in figure 10 for both studied polarizations. No anomaly is observed at the phase transition for the direction parallel to the $\boldsymbol{a}$ axis. Note that the sample becomes semi-transparent at low frequency for this polarization. No soft mode is therefore observed for this polarization, as expected since the direction is normal to that of the spontaneous polarization. Note that we disagree with the dielectric constant levels published for this polarization below 50 cm^{-1} in [14] and [15]. They actually correspond to misinterpretation of reflectivity upon the back face of the crystal and the sample holder, in the semi-transparent regime.

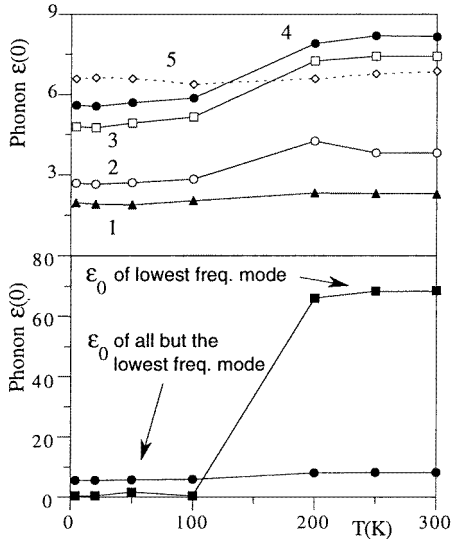

Figure 10. Comparison of the temperature dependence of the sum of oscillator strengths of infrared phonon modes for the polarizations parallel to the $\boldsymbol{a}$ axis (broken line) and $\boldsymbol{b}$ axis (full line). For the latter polarization and in the figure on top, the sum was taken without the lowest frequency mode and up to (1) ≈60 cm^{-1}, (2) ≈90 cm^{-1}, (3) ≈260 cm^{-1}, (4) ≈3500 cm^{-1}.

Figure 3 shows a much higher low-frequency reflectivity at 300 K than at 4 K for the $\boldsymbol{b}$ axis. As a consequence, the dielectric constant measured at 300 GHz shows a strong variation near the temperature of the phase transition to saturate at a high level at higher temperature. However, no clear downshift of any frequency is observed upon inspection of the temperature dependence of mode frequencies plotted for this polarization in figure 8. Conversely, to fit the reflectivity data at 200 K and higher temperatures, one has to consider a mode the existence of which is not clear below the phase transition temperature. The mode is so highly damped that it could be a relaxator equally well, as $(\gamma_{TO}/\omega_{TO}) \sim 1.8$. Koch and Happ [14] also detected such a low-frequency mode in the temperature range 203–322 K. Nevertheless, its oscillator strength above T_2 is by far the highest among all modes as shown in figure 10, and explains the behaviour of the low-frequency reflectivity, hence the dielectric constant at 300 GHz. The signature of the phase transition is also

visible in the behaviour of the oscillator strength and TO damping of some other modes, even if they negligibly contribute to ε_0, as shown in selected plots displayed in the insets of figures 8 and 9. The level of dielectric constant found at 300 GHz is much lower than the dielectric constant measured at 100 kHz near and above T_2. This difference together with the overdamped character of the lowest-frequency mode points towards the signature of relaxational mode to trigger the PE–FE phase transition rather than a soft mode. The time scale of the relaxational motions extends up to the characteristic frequency typical of very far infrared (10–50 cm^{-1}). This conclusion confirms that of [14], based on a different procedure of data treatment. The facts that (i) the relaxational mode extends up to the phonon spectral range, (ii) the oscillator strength of certain phonon modes show a signature of coupling with the order parameter of the phase transition, even in a complicated way, all strongly supports a picture of proton ordering in the FE phase and disordering in the PE phase, with the relaxational proton motions coupled with phonons.

Results of figures 2 to 10 show that very few additional modes are reported below T_2. This result is consistent with the relatively low level (2×10^{-6} C cm^{-2}, compared to 71×10^{-6} C cm^{-2} in $LiNbO_3$) of the spontaneous polarization which is observed below T_2, and the small anomalies found in the temperature dependence of x-ray diffraction [11]. It also confirms that the phase transitions involve very small atomic displacements which, in return, involve weak additional polar character (remember that only polar modes are probed by infrared). This discussion considers only vibrational modes and excludes relaxational modes, proton motions in particular. The broad species observed in the range 80–1200 cm^{-1}, together with some Fano-type interference profiles, strongly indicate that we likely face in this range a signature of coupling between proton order–disorder motions and vibrational stretching and bending modes internal to the PO_3^{3-} ions [29].

2.3. Ionic effective charges

Another advantage of infrared reflectivity spectroscopy lies in the availability of both TO and LO mode frequencies. The TO–LO splittings are a straightforward consequence of ionic effective charges $(Ze)_k$, that are the origin of instantaneous dipole moments probed by infrared radiation, via [17, 18]

$$\sum_j (\Omega_{jLO}^2 - \Omega_{jTO}^2)_\alpha = \frac{1}{\varepsilon_v V} \sum_k \frac{(Ze)_{k\alpha}^2}{m_k} \tag{5}$$

where α denotes a direction of polarization and where the summation in the right-hand side of the equation is over all atoms of mass m_k contained in the unit cell of volume V. In all displacive ferroelectrics that one of the authors (FG) has investigated in the past, a decrease of the effective charge in the direction parallel to the ferroelectric axis has been observed [17] below any PE–FE phase transition, with respect to the value found in the PE phase (see also [1]–[3]). The decrease is understood as due to the pairings of cation–anion couples that are responsible for the spontaneous polarization in the ferroelectric phase. The temperature dependence of $(1/\varepsilon_v V) \sum_k [(Ze)_{k\alpha}^2/m_k]$ is plotted in figure 11 for both polarizations studied in BPI. A net decrease of the term $(1/\varepsilon_v V) \sum_k [(Ze)_{k\alpha}^2/m_k]$ parallel to the FE $\boldsymbol{b}$ axis is observed just below the PE–FE phase transition T_2, whereas nothing similar occurs along the $\boldsymbol{a}$ axis. This is consistent with previous observations in other uniaxial ferroelectrics.

The behaviour of the effective charge has its origin in the evolution of the ionic character of the chemical bonds. An increase in the latter should result in a decrease of the observed effective charge. The increase in decreasing temperatures within the ferroelectric phase, observed in figure 11, is an indication that there is a decrease of the ionic character of some

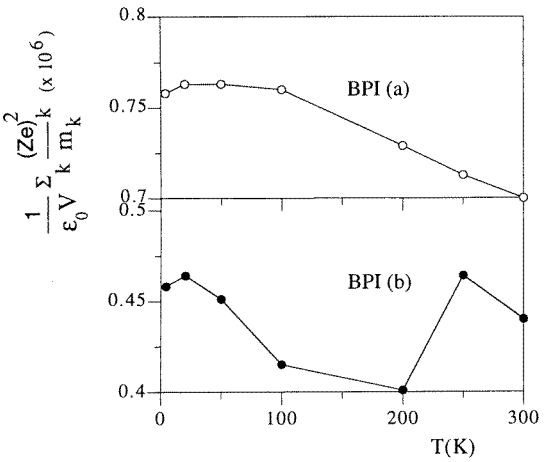

Figure 11. A comparison of the temperature dependence of BPI effective charges for $\boldsymbol{E}\|\boldsymbol{a}$ and $\boldsymbol{E}\|\boldsymbol{b}$ polarizations.

bonds. But these bonds are probably not the ones responsible for the ferroelectricity in BPI because the spontaneous polarization does not diminish in decreasing temperatures, at least until 90 K [7].

One way to explain the decrease of effective charge along the FE axis upon cooling below T_2 is to consider an increase of electronic orbital hybridization which, due to the structure and geometry of bonds may concern O–H$\cdots$O and/or P–O bonds. In addition, mode coupling phenomena mix internal modes of the betaine molecule with internal modes of the PO_3^{3-} ion, preventing the use of the method developed for tetramethyl-ammonium tetrachlocuprate [29]. Nevertheless, since the weight of Z_P^2/m_P is *a priori* much smaller than that of Z_H^2/m_H in (5) owing to the ratio of masses, it is likely that the large variation observed in figure 11, has to be primarily assigned to the hydrogen term which is dominant. Using (5) with the volume of the unit cell obtained from [9], combined with the electric neutrality, we have studied the simplified system BH_3PO_3, where B stands for the betaine molecule considered in this approximate model as a rigid entity. We are left with two equations but four unknowns ($Z_{betaine}$, Z_P, Z_H and Z_O) for each direction of polarization. We therefore investigate the evolution of Z_H and Z_O due to changes in Z_b and Z_P. The results obtained are presented in figure 12 and confirm that varying Z_b/e between 0 and 1 does not relevantly change the effective charges found for the lighter atoms H and O. In addition, we conclude that the hydrogen effective charge can be determined accurately and appears little sensitive to the values estimated for the other ions: $Z_H/e \sim 0.75$, irrespective of the assumptions made for the other contributions. Conversely, the oxygen charge is very sensitive to the input value assigned to the phosphorous charge, but for high values of Z_b and Z_P one finds Z_O/e approaching -2, which becomes physically unrealistic due to the partial hybridization inside a phosphite molecular group.

We then use the evaluation $Z_P/e \approx 2$ of the phosphorus effective charge in lead phosphate [30] in which the modes internal to the PO_4 tetrahedron are well separated from external modes due to the high mass of lead. We keep this value as a constant in our simplified model of BPI. Note that $+2$ might actually be overestimated since the formal valence of P in phosphite is only $+3$, whereas it is $+5$ in phosphate. Then, for an intermediate value of $Z_b = 0.5e$, the jump at the phase transition temperature T_2 for the polarization parallel to the $\boldsymbol{b}$ axis is thus assigned to an increase of Z_H/e from 0.67 at 200 K

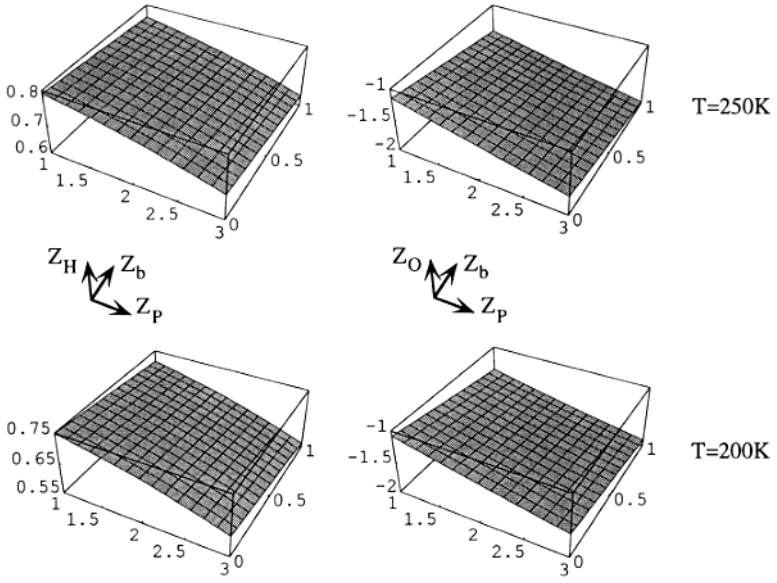

Figure 12. Evolution of effective charge of hydrogen Z_H and oxygen Z_O due to changes in effective charges of phosphorus and betaine and considering e as unit charge.

($Z_O/e = -1.51$) to 0.74 at 250 K ($Z_O/e = -1.57$). The simplest way to explain the change of $\sum Z_k^2/m_k$ on both sides of T_2 is thus to consider a small increase of hybridization with neighbour oxygen atoms of the zig-zag chains upon cooling, related to the change of average hydrogen–oxygen bond length. Note that the value found for the acid hydrogen effective charge is very large compared to the 'normal' charge found for hydrogen atoms involved in the C–H bonds. The latter may be evaluated with (5) from the sole contribution of C–H vibration modes well identified near 3000 cm^{-1}, and one finds $Z_H/e \approx 0.04$ only. This value is of the same order of magnitude as that previously found in tetramethyl-ammonium tetrachlorocuprate [29]. Whereas the error on the variation of hydrogen effective charge with temperature is small, its absolute value is only approximate, because we neglected the TO–LO splittings of modes internal to the betaine molecule. But their contribution is small, and there is no strong reason that the contribution would have a relevant variation with temperature. For the polarization along the $\boldsymbol{a}$ axis, we find $Z_H/e = 0.93$, $Z_O/e = -1.77$ (still with $Z_P/e = 2$ and $Z_B/e = 0.5$ fixed) and these values are found independent of temperature. Again, even if the acid hydrogen effective charge is slightly overestimated in this calculation due to the neglect of TO–LO splittings of modes internal to the betaine molecule, such high experimental values of Z_H justify *a posteriori* the wording 'proton', at least to some extent. Indeed, the picture we propose is a decrease of the 'protonic' character upon cooling below T_2 for the polarization parallel to the FE axis, or in other words an increase of the H–O bond hybridization mainly associated with the ordering of the protons in the O–H$\cdots$O bonds along the chains, reinforcing the conclusions obtained using other experimental techniques [10]. The mechanism of the phase transition would therefore result from the competition of H–O hybridization which tends to stabilize the FE phase and thermal amplitude of vibrations which acts again it. Finally, note that for further comparisons with calculations of electronic bands, present data are to be considered as dynamic effective charges, not static ones, *viz.* they implicitly take into account the amplitudes of the atomic vibrations.

3. Summary

The temperature dependence (4–300 K) of infrared reflection spectra of betaine phosphate single crystal is reported for the polarizations parallel to both $\boldsymbol{a}$ and $\boldsymbol{b}$ axes over the wavenumber range 10–5000 cm^{-1}. Spectra were fitted with the factorized form of the dielectric function satisfactorily. A tentative mode assignment has been proposed by comparison with the spectra of betaine phosphate, betaine arsenate, deuterated betaine phosphite single crystals and compressed betaine powder. Modes that are coupled to (supposedly broad) proton modes appear also anomalously broad. Some narrow modes appear asymmetric due to Fano-type interference phenomena. But these anomalous spectral signature show up only parallel to the $\boldsymbol{b}$ axis, only in the range 800–1200 cm^{-1}, and are found to be less marked than in betaine phosphate. Thus the change of symmetry from tetrahedron to pyramid for the phosphorus–oxygen inorganic groups is found to modify seriously the coupling mechanisms. It is confirmed that it is the basic hydrogen order–disorder mechanism that explains the critical behaviour of BPI. Additional signatures of coupling with the order parameter of the T_2 phase transition are mainly found in the temperature dependence of the oscillator strength of several modes. Finally, an estimate of the acid proton effective charges has been derived from the spectral data. The net evolution found for the polarization parallel to the FE axis in the vicinity of the T_2 phase transition may be assigned to slight change of hybridization of electronic orbitals of oxygen and acid hydrogen, although a concomitant change of P–O hybridization cannot be excluded.

Acknowledgments

The authors thank J M B Lopes dos Santos for his computational assistance and Annie Blin (CRPHT, CNRS, Orléans) and Albano Costa for technical assistance. This work was partially supported by Service Culturel Scientifique et de Coopération de l'Ambassade de France au Portugal, by Junta Nacional de Investigaçâo Cientifica e Tecnologica and by Instituto de Materiais (IMAT-nucleo IFIMUP), by Centro de Física da Universidade do Porto and by project PRAXIS/2/2.1/FIS/26/94. J Agostinho Moreira thanks Programa PRAXIS XXI for his grant BD/3192/94.

References

[1] Simon P and Gervais F 1985 *Phys. Rev.* B **32** 468
[2] Gervais F and Simon P 1987 *Ferroelectrics* **72** 77
[3] Simon P, Gervais F and Courtens E 1988 *Phys. Rev.* B **37** 1969
[4] Schildkamp W and Spilker J 1984 *Z. Kristallogr.* **168** 159
[5] Fehst I, Paasch M, Hutton S L and Braune M 1993 *Ferroelectrics* **138** 1
[6] Brückner H J, Unruh H G, Fischer G and Genzel L 1988 *Z. Phys.* B **71** 225
[7] Santos M L 1998 unpublished results
[8] Albers J, Klöpperpieper A, Röther H J and Haussühl S 1988 *Ferroelectrics* **81** 991
[9] Santos M L, Kiat J M, Almeida A, Chaves M R, Klöpperpieper A and Albers J 1995 *Phys. Status Solidi* b **189** 371
[10] Bauch H, Böttcher R and Völkel G 1993 *Phys. Status Solidi* b **179** K41
[11] Santos M L, Andrade L C R, Costa M M R, Chaves M R, Almeida A, Klöpperpieper A and Albers J 1997 *Phys. Status Solidi* b **199** 351
[12] Santos M L, Almeida A, Chaves M R, Klöpperpieper A, Albers J, Gomes-Moreira J A and Gervais F 1997 *J. Phys.: Condens. Matter* **9** 8119
[13] Fano U 1961 *Phys. Rev.* **124** 1866
[14] Koch and Happ H 1993 *Ann. Phys. Lpz.* **2** 522

[15] Ebert, Lanceros-Mendez S, Schaack G and Klöpperpieper A 1995 *J. Phys. C: Solid State Phys.* **7** 9305
[16] Baran J, Czapa Z, Drozd M K, Ilczyszyn M M, Marchewk M and Ratajczak H 1997 *J. Mol. Struct.* **403** 17–37
[17] Gervais F 1980 *Phys. Status Solidi* b **100** 337
Gervais F and Servoin J L 1981 *J. Physique Coll.* **42** C6 415
Fontana M D, Métrat G, Servoin J L and Gervais F 1984 *J. Phys. C: Solid State Phys.* **16** 483
Gervais F, Simon P, Echegut P and Calès B 1985 *Japan. J. Appl. Phys.* **24** 117
[18] Gervais F 1981 *Phys. Rev.* B **23** 6580
[19] Gervais F 1983 *Infrared and Millimeter Waves* vol 8, ed K J Button (London: Academic) pp 279–339
[20] Tsuboi M 1957 *J. Am. Chem. Soc.* **79** 1351
[21] Weast R C (ed) 1989 *Handbook of Chemistry and Physics* (Boca Raton, FL: Chemical Rubber Company)
[22] Ouafik Z 1995 *PhD Thesis* University of Paris VI
[23] Novak A 1974 *Struct. Bonding* **18** 177
Sokolov N D, Lener M V and Savl'ev V A 1990 *J. Mol. Struct.* **222** 265
[24] Blinc R and Ribaric M 1963 *Phys. Rev.* **130** 1816
[25] Moreira J A, Almeida A, Chaves M R, Mota M F, Klöpperpieper A and Pinto F to be published
[26] Moreira J A 1998 unpublished results
[27] Shildkamp W, Shäfer G and Spilker J 1984 *Z. Kristallogr.* **168** 187
[28] Courtens E and Vogt H 1985 *J. Chim. Phys.* **82** 317
[29] Gervais F and Arend H 1983 *Z. Phys.* B **50** 17
[30] Gervais F and Kaczmarek W 1983 *Z. Phys.* B **51** 137